

Design of a three-dimensional capacitor-based six-axis force sensor for human-robot interaction

Zexia he, Tao Liu*

The State Key Laboratory of Fluid Power and Mechatronic Systems, School of Mechanical Engineering, Zhejiang University, Hangzhou, 310027, China



ARTICLE INFO

Article history:

Received 13 January 2021
Received in revised form 17 June 2021
Accepted 19 June 2021
Available online 5 July 2021

Keywords:

Three-dimensional capacitor structure
Manufacturing process
Six-axis force sensor
Human-robot interaction

ABSTRACT

Multi-dimensional force sensing capability of the robot plays a critical role in its interaction with the human and environment. The six-axis force sensor as a typical representative of the multi-axis force sensor, however, has not been extensively used in the field of human-robot interaction due to its high price. A low cost, a good sensing accuracy, and a high integration level six-axis force sensor is highly desirable to create. In this paper, to weaken the crosstalk phenomenon between the six-axis and optimize the sensitivity of overall system, a 3D capacitor structure with a cross-shape configuration of the shear force sensing cell was proposed. Eight electrodes were arranged on three perpendicular planes of the Cartesian coordinate system independently. The cross-shape differential capacitor was designed to achieve the improvement of sensitivity along the shear force direction. With Polyoxymethylene (POM) selected as the substrate material, a monolithic spatial structure was manufactured using CNC technology, and then conductive copper paint was sprayed on the specific surfaces of this 3D structure. The cost-effective prototype sensor has been manufactured without the manual work and experimentally validated by comparing it with a commercial six-axis force sensor. The characteristics of the prototype were analyzed in terms of its linearity, interference error, hysteresis, time domain response, SNR, offset repeatability and time drift. Finally, to verify the instrumented six-axis force sensor further, a controlled lab test was performed to measure the interaction forces with the Baxter Research Robot in a simulated scenario.

© 2021 Elsevier B.V. All rights reserved.

1. Introduction

Recently, in extensive robotics research such as rehabilitation robot, powered lower-limb prosthesis, wearable exoskeleton, there has been a strong requirement to help the robots to interact safely with humans in unstructured environments. Indeed, accurate force sensing capability plays a vital role in physical human-robot interactions [1–7]. Especially, six-axis force sensor, due to their ability to detect six-axis force components simultaneously, is extremely important in various robot applications.

There are conventional commercial six-axis force sensors used in real applications [8]. These sensors use strain gauges as the force sensing elements. However, these commercial products are still uncommon in physical human-robot interactions because of the high cost. Previous researches reveal that the fabrication process of resistive type sensor requires well-trained operators who can bond the strain gauges to the specific surface of elastic structure pre-

cisely. Owing to this manufacturing process, commercial six-axis force sensors are very expensive to implement [9]. And this strain gauge type force sensors typically require a special purpose amplifier box for significant amplification of the change in resistance value and its correction when in use. This hampers its practical application in the physical human-robot interactions.

Meanwhile, many researchers have conducted the study on the six-axis force sensor. Typically, there are several sensing methods to measure forces and torques, including strain gauge, piezoelectric, parallel mechanism, and capacitive sensing schemes. Likewise, current researches on strain gauge type six-axis force sensor, which mainly focuses on the further optimization of the flexure elements, also had similar limitations as mentioned above [10–15]. Previous studies proposed a piezoelectric six-dimensional force sensor for the large load [16–18]. However, the piezoelectric sensors are generally suitable for measuring dynamic force, instead of static force. Furthermore, additional signal-processing devices are also required in the process of use. Yao et al. designed a six-axis force sensor based on Stewart platform [19–21]. Because of the parallel mechanism, this type of sensor was generally too large to be used in robotics research. In summary, in spite of their own advantages, the

* Corresponding author.

E-mail address: liutao@zju.edu.cn (T. Liu).

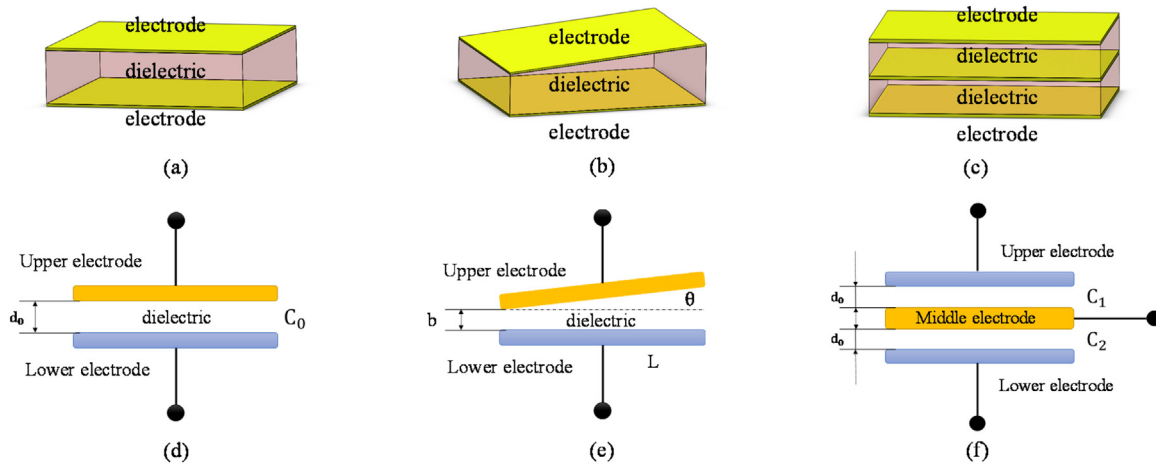


Fig. 1. Structure and working principle of capacitive-type sensing cell. 3D model of typical capacitive-type sensing cell: (a) Parallel plate capacitor. (b) Non-parallel plate capacitor. (c) Differential capacitor. Schematic cross-section of typical capacitive-type sensing cell: (d) Parallel plate capacitor. (e) Non-parallel plate capacitor. (f) Differential capacitor.

aforementioned six-axis force sensors have some defects, which restricts their wide application in the field of physical human-robot interaction. In order to broaden their use scope, a low cost, a high integration degree, and a good sensing accuracy are highly desirable to create.

Currently, there has been considerable interest in exploiting the capacitance change to measure multi-dimensional force [4,6,9,22–25]. Capacitive type multi-axis force sensor is simple in structure, small in volume, and equally good in performance. It is the most promising to become an optimal sensing scheme used for human-robot interaction. A novel commercial capacitive six-axis force sensors (DynPick) have been developed by WACOH-TECH corporation in japan [26]. Although cost reductions were realized by simple sensing principle and mass production, the price of commercial capacitive six-axis force sensor for the large load (DynPick: WEF-6A1000-30 series) was still high. Furthermore, in the literature [4,9,23], capacitive type force sensing method was an alternative to the conventional strain gauge type six-axis force sensor for robotic applications. These sensors were mainly used for the measurement of tiny forces, such as surgical robots. The existing force sensing ranges were very small. In addition, the sensitivity of the shear force sensing structure was not too high. To sum up, at this stage, the capacitive type six-axis force sensor had some characteristics: i) Commercial capacitive six-axis force sensors with a wide measuring range are still too expensive, which restricts its uses in the field of human-robot interaction. And the research on the capacitive six-axis force sensor for large load has not been reported yet. ii) The in-plane configuration of the positive electrodes causes the coupling effect and the low sensitivity along the shear force direction, which seriously impacted the isotropic property of the six-axis force sensor. Given these, it is meaningful to achieve a capacitive type sensor with a larger sensing range at a lower cost. Moreover, the novel capacitor structure need to be explored to optimize overall system sensitivity with respect to the six directions and reduce the coupling effect between the six-axis.

To address these issues, in this paper, we present a cost-effective six-axis force sensor for the large load in the human-robot interaction field. To achieve a better decoupling effect and isotropic property, a 3D capacitor structure with a cross-shape configuration of the shear force sensing cell was proposed. Eight sensing electrodes were arranged on three perpendicular planes of the Cartesian coordinate system independently to weaken the couple effect to the maximum extent. Meanwhile, the cross-shape differential capacitors along the shear force direction were designed to

achieve the improvement of the sensitivity, which can optimize the isotropic property of overall system. With Polyoxymethylene (POM) as the substrate material, a monolithic spatial sensing structure was manufactured using computer numerical control (CNC) technology and spraying technology. The proposed design concept was implemented by manufacturing a prototype sensor. Performance evaluations have been performed by comparing it with a commercial six-axis force sensor. Furthermore, a controlled lab test was performed with the Baxter Research Robot to validate the instrumented six-axis force sensor in a simulated scenario.

2. Sensing principle

2.1. Working principle of capacitive-type sensing cell

In general, a parallel plate capacitor sensor is composed of two parallel conductive electrodes and a dielectric material between them. The capacitive type force sensing method can be used to measure force and torque. As illustrated in Fig. 1(a) and (d), the capacitance of this capacitor can be calculated by

$$C_0 = \frac{\varepsilon \varepsilon_0 A}{d_0} \quad (1)$$

where ε is the relative dielectric constant in dielectric and ε_0 represents the permittivity of vacuum. d_0 and A are the vertical distance between the two parallel conductive plates and the overlapping area of the conductive plates, respectively. Thus, a small variation of the vertical distance Δd between parallel conductive plates caused by a normal force can be sensed by the capacitance variation ΔC . In this case, the relative change in capacitance can be calculated by

$$\frac{\Delta C_d}{C_0} = \frac{\Delta d}{d_0} [1 + \frac{\Delta d}{d_0} + \left(\frac{\Delta d}{d_0}\right)^2 + \left(\frac{\Delta d}{d_0}\right)^3 + \dots] \approx \frac{\Delta d}{d_0} \quad (2)$$

Assuming that $\frac{\Delta d}{d_0} \ll 1$, $\frac{\Delta C_d}{C_0} \approx \frac{\Delta d}{d_0}$. In addition, another case is the non-parallel plate capacitor caused by torque. As depicted in Fig. 1(b) and (e), this structure can also be used to measure the moment applied to the conductive plate. In this scenario, the capacitance of this type capacitor can be calculated by

$$C = \frac{\varepsilon_0 A}{b} \cdot \left(1 - \frac{L \cdot \theta}{2b}\right) \quad (3)$$

where θ represents the angle between conductive plates and b is the distance between the narrow ends of two conductive plates. L

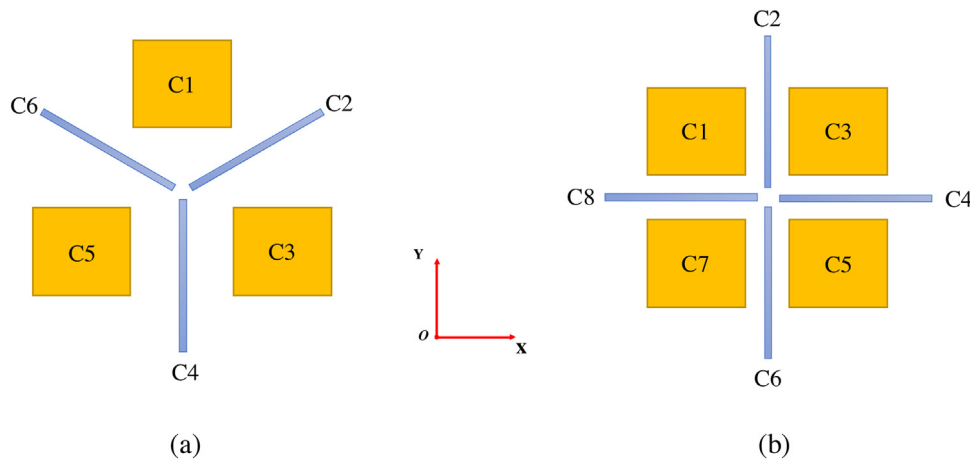


Fig. 2. Spatial arrangement of force sensing cells. (a) The Y-shape configuration. (b) The cross-shape configuration.

is the length of the lower conductive plate. To sum up, the capacitance relies on the distance between the two parallel conductive plates. On the other hand, a small variation of the overlapping area ΔA caused by a shear force can also be detected by the capacitance variation ΔC . However, in this configuration, this shear force sensing method is less sensitive, which is rarely used in practical applications.

In this study, to increase the sensitivity of shear force sensing, a gap-alterable differential capacitor sensor is designed, as shown in Fig. 1(c) and (f). Specifically, the upper and lower electrodes of the differential capacitance sensor are fixed, which is called the static plate, and the middle electrode is the moving plate. When the moving distance of the middle plate is Δd , the gap of the capacitor C1 becomes $d_0 - \Delta d$, the other one (capacitor C2) becomes $d_0 + \Delta d$. Thus, the total change in capacitance can be expressed by

$$\Delta C = C_1 - C_2 = C_0 [2 \frac{\Delta d}{d_0} + 2 \left(\frac{\Delta d}{d_0} \right)^3 + 2 \left(\frac{\Delta d}{d_0} \right)^5 + \dots] \quad (4)$$

The relative change in capacitance can be calculated by

$$\frac{\Delta C_d}{C_0} = 2 \frac{\Delta d}{d_0} [1 + \frac{\Delta d}{d_0} + \left(\frac{\Delta d}{d_0} \right)^2 + \left(\frac{\Delta d}{d_0} \right)^4 + \dots] \approx 2 \frac{\Delta d}{d_0} \quad (5)$$

Assuming that $\frac{\Delta d}{d_0} \ll 1$, $\frac{\Delta C_d}{C_0} \approx 2 \frac{\Delta d}{d_0}$. Compared with (2), it can be seen that after adopting differential mode, the sensitivity of the capacitance sensor is doubled. Meanwhile, the relative nonlinear error is reduced by order of magnitude. In this study, these two kinds of configurations of parallel conductive plates were used to sense multi-dimensional force.

2.2. Measuring principle of the 3D capacitive six-axis force sensor

To measure the 6-axis force component, at least six force sensing cells should be required. In this study, the normal force sensing cells (Orange Square) were placed in the horizontal plane. Moreover, all the shear force sensing cells (Blue Rectangle) were vertically positioned, which can help to greatly improve the detecting sensitivity for the shear force component in comparison with previous researches [4,9,23]. Typically, there are two kinds of layout methods for force sensing cells in the 3D space. As shown in Fig. 2(a), there are six sensing cells symmetrically placed at regular intervals (60 degree) on the board. Three sensing cells (C1, C3, C5) placed in the horizontal plane was to detect the normal force component. Another three sensing cells (C2, C4, C6) lied on the vertical plane to measure the shear force component. However, the Y-shape configuration of shear force sensing cells causes the influence by the arbitrary tangential force to the shear force sensing cells. That is,

the shear force sensing cells (C2, C6) were simultaneously affected by all the shear force components (F_x, F_y), which causes the cross effect.

To weaken the effect further, the cross-shape configuration of shear force sensing cells was specifically designed as shown in Fig. 2(b). In this spatial structure, the couple effect between the six-axis has weakened to the maximum extent. Four normal force sensing cells in the horizontal plane only detects the normal force/torque components. Especially, two shear force sensing cells (C4, C8) in the vertical plane were designed to measure the shear force along the y direction. And in another direction that's perpendicular to this vertical plane, other sensing cells were used to measure the shear force (F_x). Thus, the couple effect between these shear force components decreases with the proposed cross-shape arrangement. In this case, the structure's coupling effect becomes weaker, which is superior to the Y-shaped layout of shear force sensing electrodes. In our study, the cross-shape configuration of shear force sensing cells was adopted in the design.

As mentioned above, eight sensing cells were arranged on three perpendicular planes of the Cartesian coordinate system independently. Fig. 3 illustrates the sensing principles of the six-axis force sensor. Based on the spatial layout of positive electrodes in the 3D space, eight capacitance sensing cells are created. That is four normal force sensing cells and four shear force sensing cells. The capacitance change of the eight force sensing cells was sensed to detect the six-axis force. As displayed in Fig. 3(a), the four shear force sensing cells (C2, C4, C6 and C8) can be used to obtain F_x , F_y , and M_z . Here, the differential capacitors were exploited to increase the sensitivity along the shear direction. As displayed in Fig. 3(b), the four normal force sensing cells (C1, C3, C5 and C7) can be transformed into F_z , M_x , and M_y similarly. As expressed above, the six-dimensional force can be detected as follows:

$$\begin{aligned} \Delta C_{fx} &: C_2 - C_6 \\ \Delta C_{fy} &: C_4 - C_8 \\ \Delta C_{fz} &: C_1 + C_3 + C_5 + C_7 \\ \Delta C_{mx} &: C_5 + C_7 - C_1 - C_3 \\ \Delta C_{my} &: C_3 + C_5 - C_1 - C_7 \\ \Delta C_{mz} &: C_2 + C_4 + C_6 + C_8 \end{aligned} \quad (6)$$

where ΔC_{ij} is the capacitance change that detects the six-axis force component, respectively. C_i is the measured capacitance value of the eight force sensing cells. In order to acquire the applied six-dimensional force, mathematical relations between the capacitance change and the applied load were derived. Specifically, due to

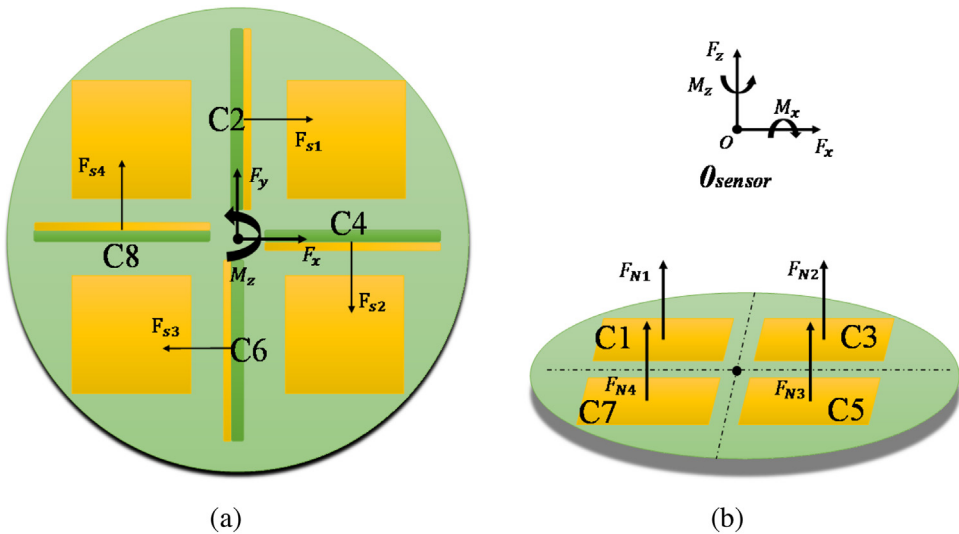


Fig. 3. Measuring principle of the six-axis force sensor. (a) In the case of shear forces. (b) In the case of normal forces.

the nonlinearity phenomenon of the capacitive sensing principle, multivariate second-order polynomials were used to fit the nonlinear relationship. The relationship can be expressed in the matrix form as follows:

$$\mathbf{F}_{6 \times 1} = T_{6 \times 12} * \Delta \mathbf{C}_{12 \times 1}$$

$$\begin{pmatrix} F_x \\ F_y \\ F_z \\ M_x \\ M_y \\ M_z \end{pmatrix} = T_{6 \times 12} * \begin{pmatrix} \Delta C_{fx} \\ \Delta C_{fy} \\ \Delta C_{fz} \\ \Delta C_{mx} \\ \Delta C_{my} \\ \Delta C_{mz} \\ \Delta C_{fx}^2 \\ \Delta C_{fy}^2 \\ \Delta C_{fz}^2 \\ \Delta C_{mx}^2 \\ \Delta C_{my}^2 \\ \Delta C_{mz}^2 \end{pmatrix} \quad (7)$$

$\mathbf{F}_{6 \times 1}$ is the actual applied six-axis force vector, and $\Delta \mathbf{C}$ is the capacitance data. It has 12 inputs: the capacitance variation values and the squares of those data. A calibration matrix T transforms the capacitance variation values into the six-dimensional force. Furthermore, the normalized calibration matrix can be obtained by applying individually the rated magnitudes for the six force components.

2.3. Design of the 3D capacitor for six-axis force sensor

In previous studies [4,9,23], all the positive electrodes are distributed in the same horizontal plane. This in-plane configuration of the positive electrodes causes data interference between the 6-axis and low sensitivity of shear force sensing, which seriously impacted the isotropic property of the six-axis force sensor. In this study, to reduce the crosstalk phenomenon and optimize overall system sensitivity with respect to the six directions, a desired spatial layout of positive electrodes in 3D space was proposed, as illustrated in Fig. 4(a). Eight electrodes were arranged on three perpendicular planes of the Cartesian coordinate system independently. More-

over, the layout of four electrodes in the vertical plane looks like a cross shape, forming two differential capacitance sensors. In comparison with the method by using the fringe effect between two orthogonal electrodes, this arrangement greatly increased the sensitivity along the shear force direction [4,9,23], which can optimize the isotropic property of overall system. There is also one major obstacle that the previous manufacturing process cannot make the 3D substrate structure. Thus, a manufacturing process was created to achieve this desired spatial structure, which previous researchers cannot do. In a word, with the proposed 3D shape substrate structure and corresponding manufacturing process, the desired 3D capacitor for the six-axis force sensor was achieved.

As for the designed 3D capacitor, it was mainly composed of a sensing board and a grounded plate, as displayed in Fig. 4(b). The sensing board contains four square electrodes and four strip electrodes, which were used as positive electrodes. Four square electrodes are placed on the horizontal plane of the circular plate, and four strip electrodes lie on the vertical plane of the beams. Meanwhile, the negative electrode of the capacitor was implemented with a common grounded plate. The 3D capacitor structure was realized just by assembling the manufactured sensing board with the common grounded plate. In this configuration, two types of capacitors (Parallel plate capacitor, Differential capacitor) mentioned above were generated to sense the normal forces and shear forces, respectively. On the one hand, the gap-alterable capacitive type sensor distributed on the horizontal surface was considered as the normal force sensing element. As displayed in Fig. 5, it was composed of the square electrode and grounded plate. A gap of air between the parallel electrodes acts as the dielectric. In the case of the applied normal force or moment, the distance d_N between parallel electrodes changes. Then, the displacement can be measured by sensing the change of capacitance. On the other hand, the gap-alterable differential capacitive sensor distributed on the vertical surface was taken as the shear force sensing element. Each capacitor of the differential sensor was composed of the strip electrode and the common grounded electrode. One differential capacitors (C_4, C_8), which are perpendicular to the x -axis of the sensor, are used to measure F_y component. The other ones (C_2, C_6), which are perpendicular to the y -axis of the sensor, are used to measure F_x component. Furthermore, the bottom surface of the grounded plate is wider than the square electrode in the sensing board to ensure that the capacitance of normal force sensing cells is not influenced by shear displacements. And its vertical surfaces are smaller than

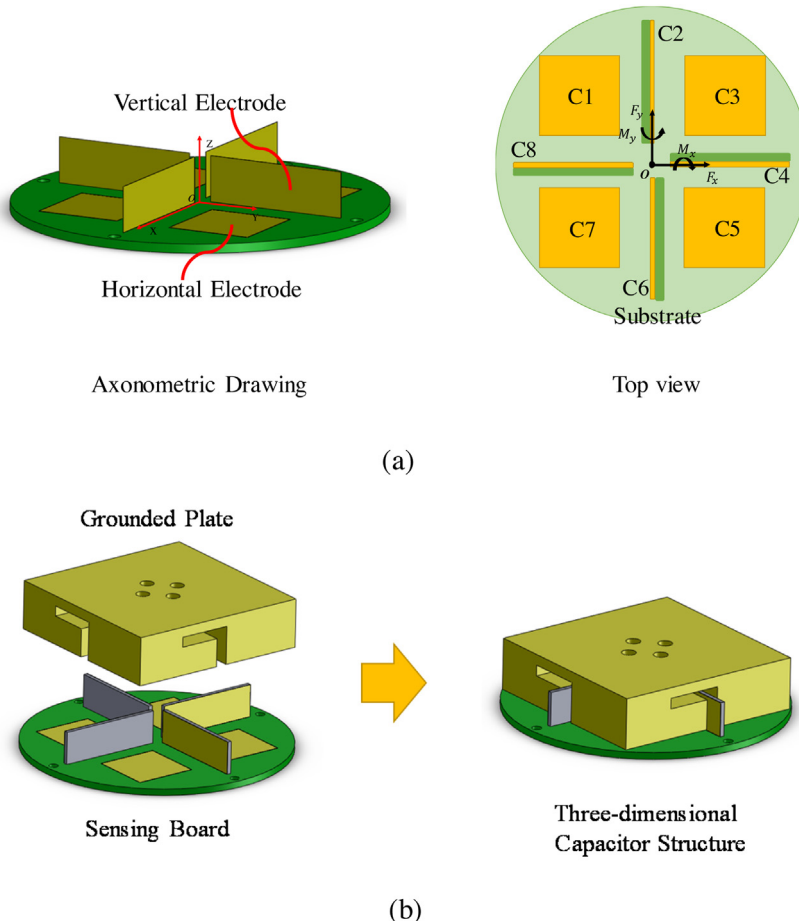


Fig. 4. Structure of the proposed 3D capacitor. (a) Spatial layout of positive electrodes in the 3D space. (b) Assembly diagram of the 3D capacitor.

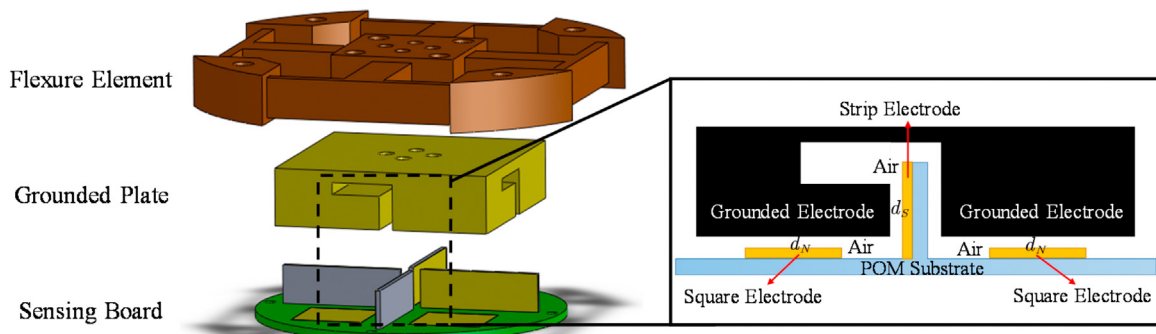


Fig. 5. Drawing of partial enlargement of the 3D capacitor.

the strip electrode to guarantee that the capacitance of the differential capacitor is not affected by normal displacements.

In this study, a processing technology was adopted to manufacture the 3D capacitor. POM material, also known as Polyoxymethylene, is an engineering thermoplastic widely used in precision parts. It was chosen as the material for the substrate of the sensing board due to its high stiffness, higher insulation, and excellent dimensional stability. This material was easy to be machined into a 3D structure by using CNC technology. As shown in Fig. 6, the manufacturing process of the 3D substrate is performed in two steps. First, the solid bar stock made of POM material is machined using a high precision CNC machining center to achieve the desired 3D substrate. Second, conductive copper paint was then sprayed on the specific surfaces of this structure to achieve the

desired spatial layout of positive electrodes. The eight electrodes were implemented with the thin copper films covered in the POM material using the spraying technology. The four square electrodes and four strip electrodes were distributed on the horizontal surface and vertical surface of this board, respectively. The entire manufacturing process of the sensing cell requires no manual work, which enables ease of manufacturing and reduces its production costs.

3. Design and development

3.1. Design of capacitive six-axis force sensor

Based on the sensing principle mentioned above, the proposed capacitive type six-axis force sensor was designed. As illustrated in

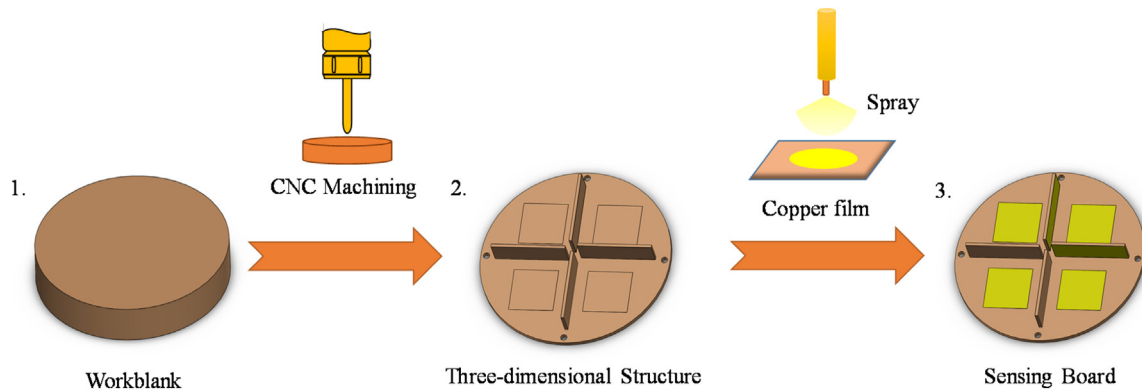
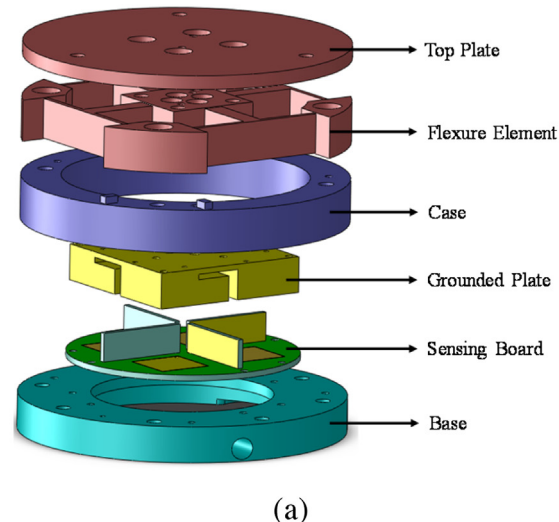
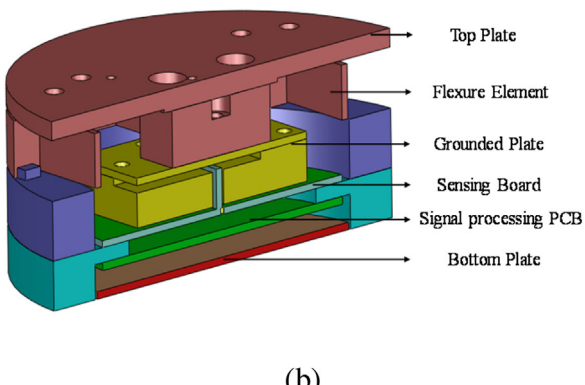


Fig. 6. A novel manufacturing process of the 3D capacitor structure.



(a)



(b)

Fig. 7. Mechanical parts of the proposed sensor. (a) Exploded view. (b) Section view.

Fig. 7, the mechanical parts of the prototype sensor are mainly composed of top plate, flexure element, grounded plate, case, base part and bottom plate. The top plate is the force receiving part that the external force/torque is applied to. The flexure element is the force sensing part, which functions as a spring to transduce the applied load into a displacement. Furthermore, the flexure element was the cross beam type elastic body, which contains four cross elastic beams and four compliant beams. The grounded plate was suspended from the movable part of the flexure element. It generates eight air gaps between its surfaces and eight electrodes of the sensing board. When external load is applied to the surface of the top

Table 1
Mechanical specifications of the developed sensor.

Quantity	Value	Unit
Diameter	90	mm
Height	39	mm
Weight	350	g
F_z	± 1000	N
F_x/F_y	± 500	N
M_x/M_y	± 45	Nm
M_z	± 45	Nm

plate, the flexure element deforms. This causes a relative displacement of the grounded plate. The capacitance of eight capacitors varied in response to the movement of the grounded plate. Thus, six-axis force sensing can be achieved by using the capacitance variation of eight capacitors. Besides, two boards are fixed to the sensor frame. The sensing board (upper board) contains eight electrodes, which makes capacitors as mentioned in earlier section. The signal processing PCB (lower board) incorporates signal processing electronics, which was used to measure capacitance data and then transmit them to the upper system. The wires are connected to the signal processing circuit of the lower PCB.

Based on the analyses mentioned above, all the mechanical parts were fabricated via conventional machine works. The photographs of the manufactured mechanical parts were shown in **Fig. 8**. Then the proposed prototype sensor was assembled, as illustrated in **Fig. 9**. It incorporates the measurement circuit internally, which is structurally simple and compact. Compared with conventional sensors, this sensor has the apparent advantage that it does not require an external device such as the signal amplifier. The force sensing ranges were defined considering the application scenarios, as shown in **Table 1**. Also, the physical dimension of the prototype sensor was summarized. The prototype sensor is lightweight: 350 g. And it has a radius of 90 mm, a height of 39 mm.

The design of capacitors largely depends on the tradeoff between the size and sensitivity of the sensor. The capacitors need to be sensitive enough in various robot applications, while maintaining the minimization of dimension. Thus, four square electrodes with a size of $10 \text{ mm} \times 10 \text{ mm}$ and four strip electrodes with a size of $5 \text{ mm} \times 27 \text{ mm}$ were designed into the sensing board. These eight electrodes were implemented with thin copper films by using a novel manufacturing technology mentioned in the earlier section. **Fig. 10** presents the custom designed 3D capacitor structure with eight electrodes of the normal and shear force sensing elements. Based on the general machining technology, the distances d_N and d_S shown in **Fig. 8** are set as 0.3 mm and 0.3 mm separately.

According to the above-mentioned analysis, from **Fig. 11**, we can see that the capacitance changing curves of these two type capacitors, which is shown by the red solid line. X-axis is the plate distance

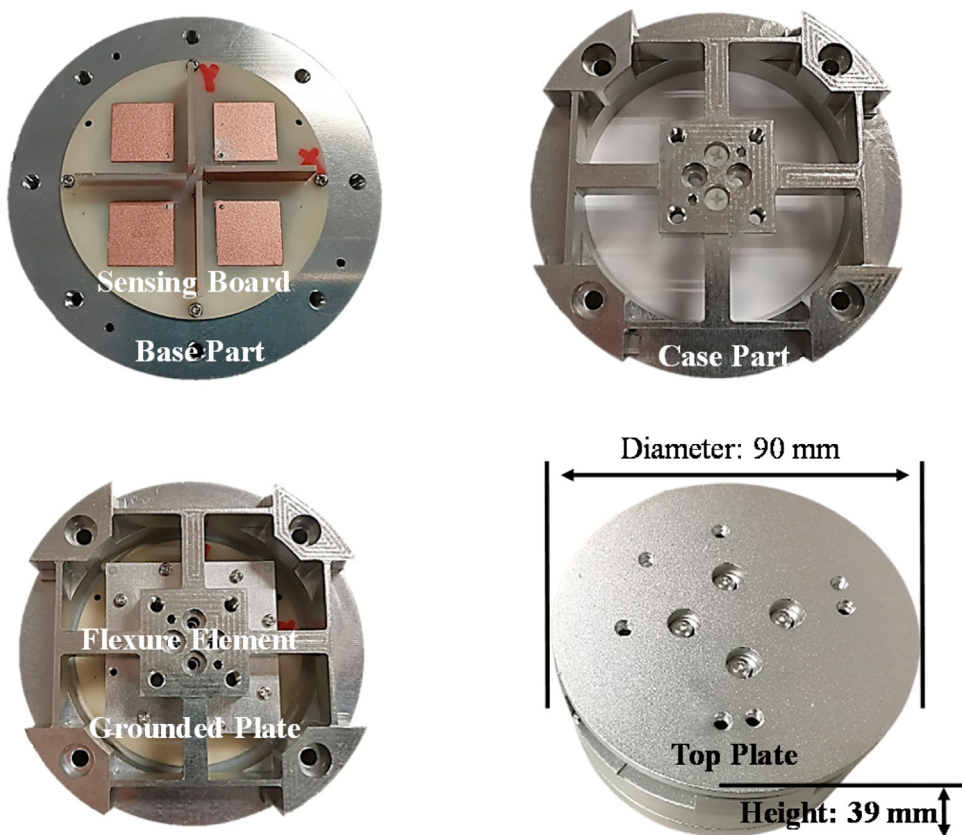


Fig. 8. Actual pictures of the manufactured mechanical parts.

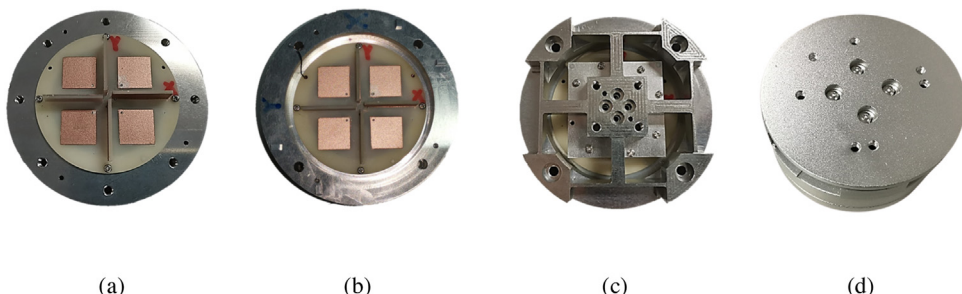


Fig. 9. Assembly process of the developed prototype sensor. (a) Base part assembled with the Sensing board. (b) Further assembled with the case part. (c) Assembled with the flexure element and grounded plate. (d) Fully assembled prototype sensor.

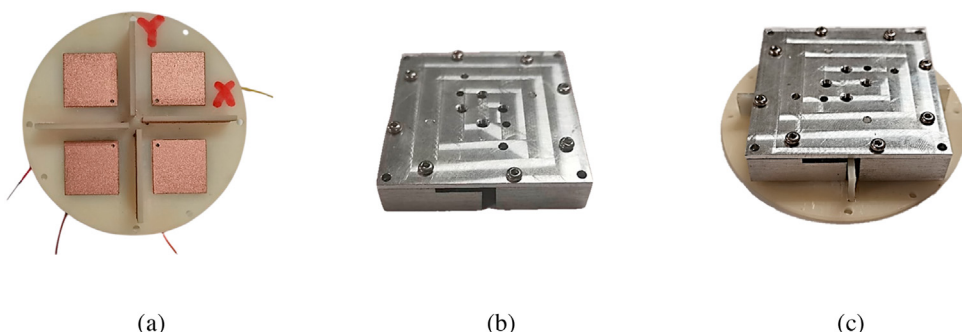


Fig. 10. Actual pictures of the developed 3D capacitor structure. (a) Sensing Board. (b) Grounded plate. (c) 3D capacitor structure.

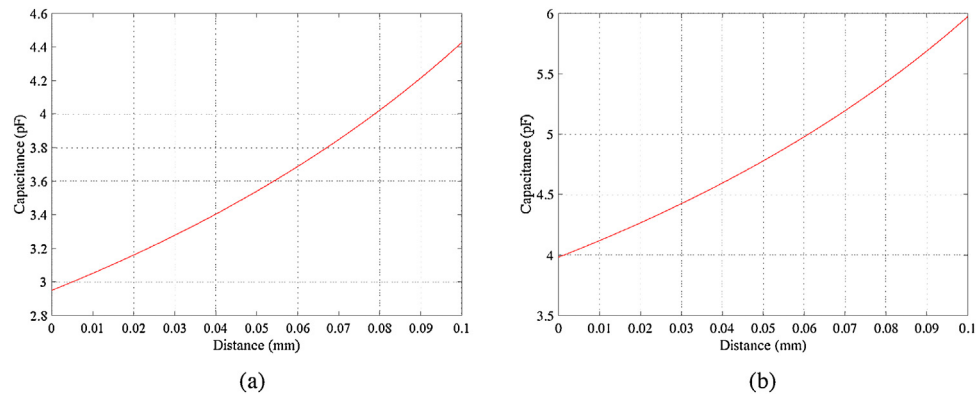


Fig. 11. (a) The capacitance variation curve of the designed normal force sensing cell. (b) The capacitance variation curve of the designed shear force sensing cell.

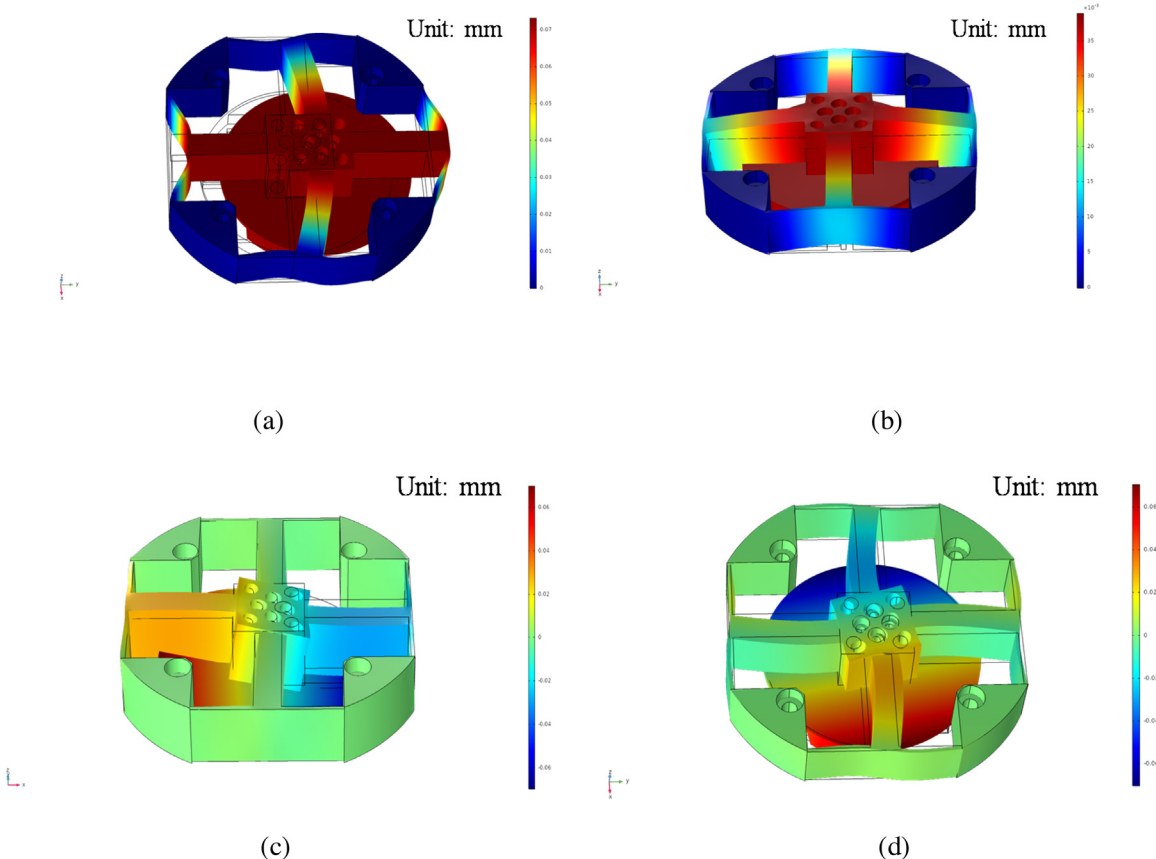


Fig. 12. Finite element analysis of the capacitive six-axis force sensor. (a) Loading with an axial force $F_y = 500$ N. (b) Loading with a radial force $F_z = 1000$ N. (c) Loading with a bending moment $M_y = 45$ N*m. (d) Loading with a torsional moment $M_z = 45$ N*m.

and Y-axis is the capacitance (pF). The analysis of the capacitance variation determines the ideal displacement of the flexure element, which is taken into account in the structural design.

3.2. Finite element analysis of capacitive six-axis force sensor

In this study, the property of the capacitive six-axis force sensor was optimized with the structural parameters of the elastic body. Typically, the flexure element was the classical cross beam type elastic structure. It was composed of outer frame, central mass, elastic beams, and compliant beams. The isotropy property of the sensor is determined by the geometrical parameters of the elastic body as shown in Table 2. Then finite element analysis (FEA) was performed to determine its optimal geometric parameters. Due to

Table 2
Parameters of the flexure element.

	Length(mm)	Width(mm)	Height(mm)
Central mass	20	20	16
Cross elastic beams	29	7.5	15
Compliant beams	41	1	15

the symmetric structure, only the four situations (F_y , F_z , M_y , and M_z) of the flexure element under a given load were analyzed here. The maximum values for F_y , F_z , M_y , and M_z were 500 N, 1000 N, 45 N*m, and 45 N*m. The material composing the elastic structure was Aluminum alloy 7075, which has tensile yield strength of 503 MPa and a modulus of elasticity of 71.7 GPa. As shown in Fig. 12, to

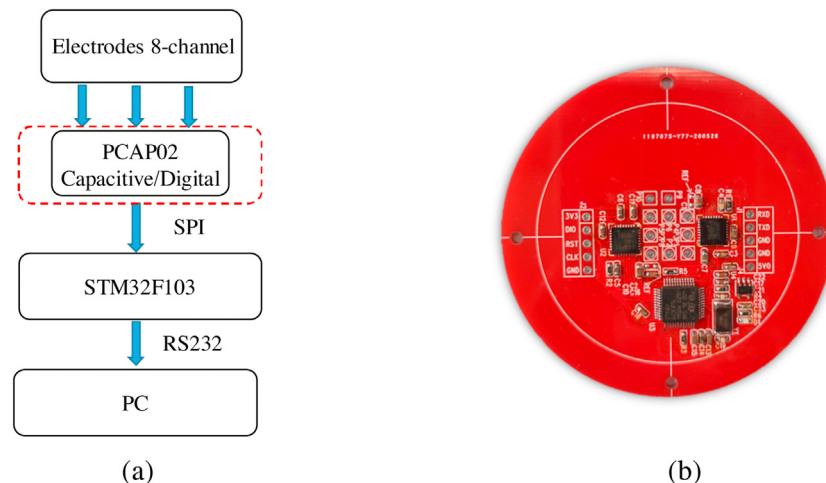


Fig. 13. (a) Schematic diagram of the capacitance measuring circuit. (b) Actual picture of signal processing PCB.

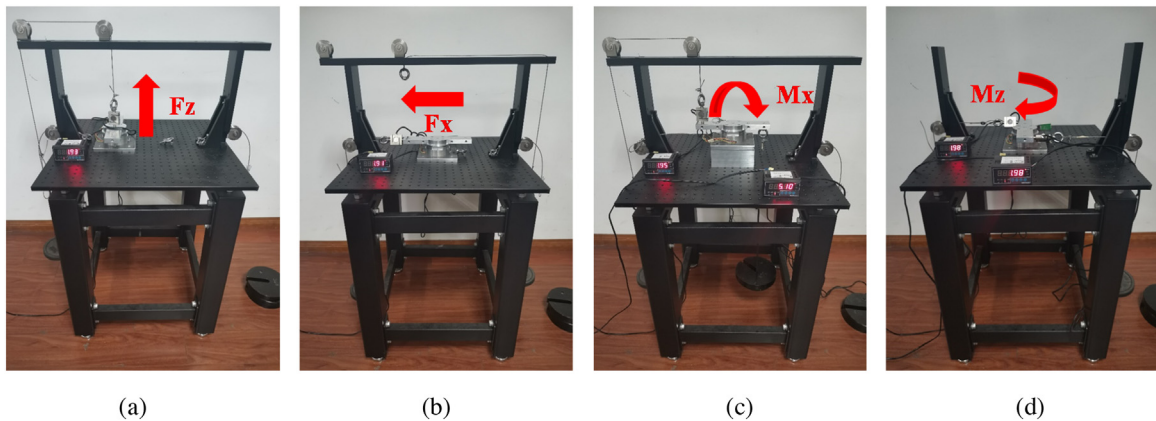


Fig. 14. Experimental setup for the calibration and evaluation of the prototype sensor. (a) Loading test for pure F_z . (b) Loading test for pure F_x . (c) Loading test for pure M_x . (d) Loading test for pure M_z .

analysis the capacitive response of the six-axis force sensor, rating force or torque component in each direction was applied to origin of the sensor's coordinate system. The maximum deformations are set as 0.068 and 0.071 mm at the normal and shear force sensing cells, respectively. As Uchiyama et al. pointed out in previous studies [27,28], the smaller the condition number, the better isotropy the structure has. The sensor has a better measuring precision. And the condition number of the normalized calibration matrix as a performance index needs to be as close as possible to 1. Thus, in order to get an optimal isotropic structure at the design stage, we updated the dimensional parameters of the elastic body based on simulation results repeatedly. Finally, in this work, the optimal parameters of the flexure element are given in Table 2.

3.3. Design of the high precise capacitance measurement system

Fig. 13 shows the high precise capacitance measuring system. In this study, a high precise capacitance to digital converter (CDC) chip with integrated digital signal processor is specially adopted to measure the capacitance data. More specifically, two CDC chips (pcap02, ACAM) and a microcontroller chip (STM32F103 series, ST) are placed on the signal processing PCB. In comparison with the previous CDC chip (AD7147, Analog Devices), this chip has a better-performing measurement accuracy [4,9,22,23]. The chip has a maximum measurement rate of 500 kHz and a 17-bit resolution.

It covers a wide capacitance input range from 1 pF to 100 nF easily. Additionally, compensation of internal and external stray capacitance is implemented while measuring. In the board, the digitized capacitance data are transmitted to the MCU chip through an SPI communication interface. Then the signal processing PCB sends the digitized data to the computer through serial communication.

4. Experimental validation

4.1. Experimental setup and calibration process

Due to the machining tolerance and assembly error of the prototype sensor, there is a certain gap between the actual and theoretical characteristics of the prototype sensor, which inevitably leads to the measurement error. Thus, it is necessary to obtain accurate force and torque readings via a static calibration process. As shown in Fig. 14, an experimental setup was specially designed to calibrate the manufactured prototype sensor. This setup was composed of a load frame, wire rope, high-precision weight, guide pulley, load cell and loading rod. In the experiment, the weights were connected to the loading rod by wire rope and guide pulley. Thus, the loading force was generated by the high-precision weight. In order to achieve the accurate loading of multi-dimensional forces, load cells were connected between the loading rod and the weight. The readings of the load cell were considered as the real

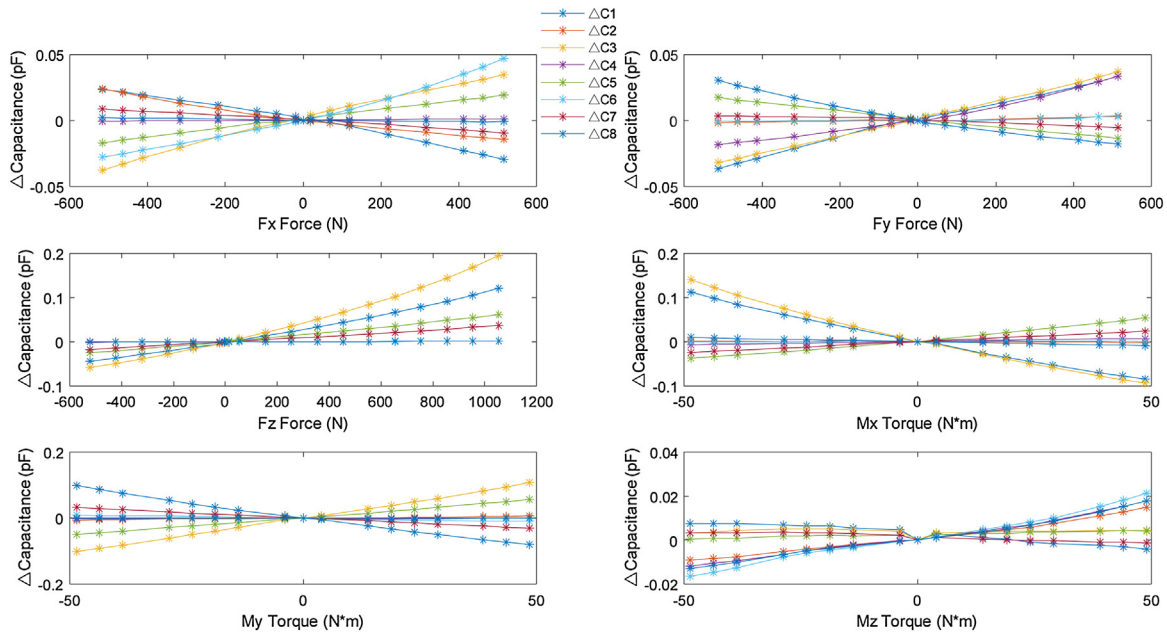


Fig. 15. Capacitance measurement results versus actual force loads in F_x -direction, F_y -direction, F_z -direction, M_x -direction, M_y -direction, M_z -direction.

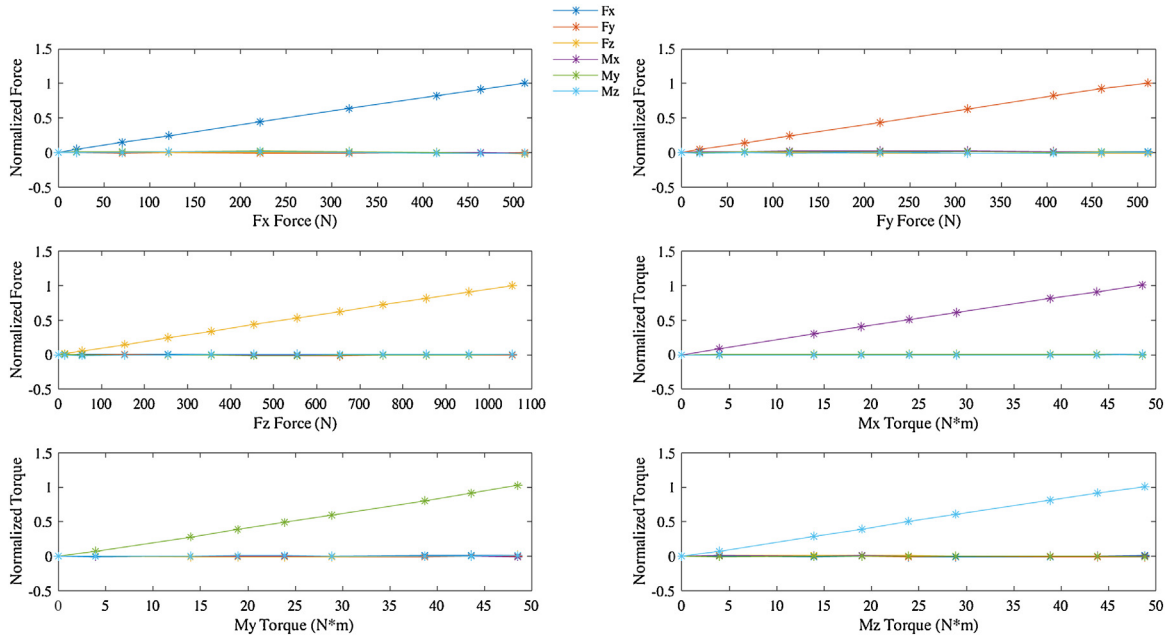


Fig. 16. Static responses of the prototype with respect to external pure force/torque input.

forces applied to the prototype sensor. This calibration procedure consists in applying the six-dimensional force to the manufactured sensor. The digitized capacitance data were recorded with the applied each six-axis force. In order to ensure the accuracy of the calibration test, each direction was loaded and unloaded cycle 3 times repeatedly. And the load was applied alone in each axis. According to the type of the applied load, the calibration setup has four loading configurations. Fig. 14(a) shows the application of the force F_z by adding the weights on the sensor. The experimental setup shown in Fig. 14(b) is used to create forces along the F_x and F_y directions. The couples M_x and M_y are also applied to the prototype sensor as shown in Fig. 14(c). In the case of M_z , the configuration shown in Fig. 14(d) is used.

4.2. Calibration results

By using the experimental setup mentioned above, a force (F_z) ranging from -500 to 1000 N was applied to the manufactured sensor. And two forces (F_x and F_y) were applied ranging from -500 to 500 N. Likewise, three couples (T_x , T_y and T_z) were applied ranging from -45 to 45 Nm. The force was exerted by adding and removing the weights in each direction. During the loading test, the capacitance values from the developed sensor were obtained. For each applied force, the mean values of the measured capacitances were calculated to eliminate the disturbance of the random error.

When applying the force or torque component in the six-axis direction individually, the output capacitance value of capacitive

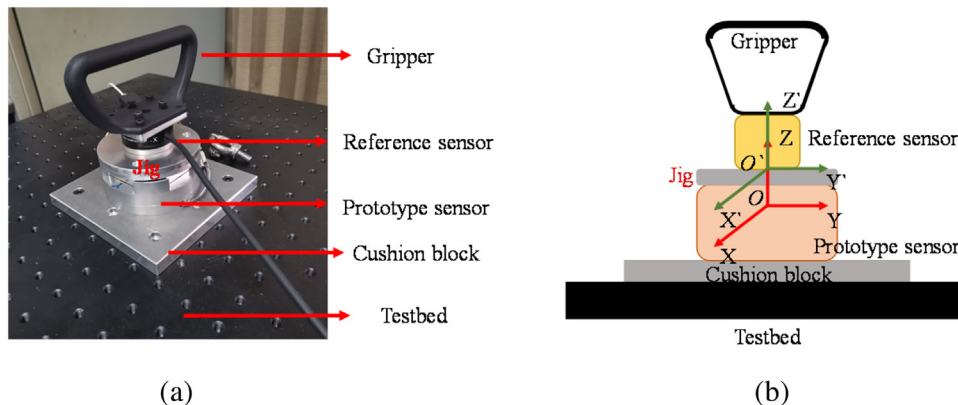


Fig. 17. Evaluation setup used to verify the prototype sensor. The prototype sensor and a commercial sensor are connected in series. (a) Actual pictures of the evaluation setup. (b) Schematic diagram of the evaluation setup.

sensing cell can be obtained. Fig. 15 shows the changes in the capacitance of the eight capacitors when each 6-axis force component is applied. The x-axis of this figure represents the input load, and the y-axis stands for the capacitance change. Then, based on the sensing principles of the six-axis force sensor, the six-dimensional force was calculated using the capacitance change. A second-order polynomial model was used for the calibration function. The relationship between the capacitive data and the six-axis force components can be expressed as mentioned in earlier part:

$$T \cdot \begin{bmatrix} \Delta C_{fx} & \Delta C_{fy} & \Delta C_{fz} & \Delta C_{mx} & \Delta C_{my} & \Delta C_{mz} & \Delta C_{fx}^2 & \Delta C_{fy}^2 & \Delta C_{fz}^2 \\ \Delta C_{mx}^2 & \Delta C_{my}^2 & \Delta C_{mz}^2 \end{bmatrix}^T \quad (8)$$

Based on the linear least squares method, each element of the calibration matrix T is derived as follows:

-8938.72	165.80	-109.51	-164.92	523.73	-1068.60	-10033.65	4640.83	-234.12	-116.06	103.29	3665.93
354.41	9480.97	-361.99	-739.49	-10.77	143.70	955.93	-4921.68	-49.50	-5.35	77.58	-1309.62
564.20	-559.43	4359.23	2194.76	-644.24	589.29	7215.60	7546.70	-932.39	-924.85	-396.12	-8343.35
1.90	67.64	102.72	222.19	-19.90	-2.25	-205.90	-174.67	43.26	14.70	-6.35	-154.76
64.19	36.01	-47.09	-29.55	179.70	-30.84	12.68	-230.38	-24.46	-18.94	12.58	35.89
227.16	-52.80	-19.13	2.83	3.14	902.32	-3995.18	-5594.11	7.60	21.08	50.90	-2588.62

4.3. *Static response*

The static characteristics of the manufactured sensor were investigated by using the same experimental setup. The single directional force was applied in each axis, which was also based on a pulley-weight method. Fig. 16 illustrates the static response of the prototype in the positive direction of each force component. The X-axis of the figures represents the applied force or torque. In order to evaluate the force and torque components in the equivalent standard, the Y-axis of the figures is normalized by maximum values of sensing range. Ideally, the slope of the straight line representing the principal direction force component should be 1. And the rest output signals in other directions should be 0. The experimental results show that the coupling direction's force components are near zero curve, which indicates the interference errors are tiny.

Table 3 summarizes the static characteristics of the prototype sensor. As can be seen, the linearity errors in F_x , F_y , F_z , M_x , M_y , M_z direction are 0.93 %F.S., 2.01 %F.S., 0.62 %F.S., 1.76 %F.S., 1.52 %F.S., and 1.58 %F.S., respectively. The maximum linearity error of the sensor is 2.01 %F.S. in the F_y direction. Then the maximum interference errors for F_x , F_y , F_z , M_x , M_y , M_z directions are 1.95 %F.S., 2.01 %F.S., 1.58 %F.S., 1.51 %F.S., 1.62 %F.S., 1.47 %F.S., respectively. All the interference errors of the sensor are almost not more than 2.00 % F.S.. From the experimental data, an average hysteresis error was

Table 3
The main performance indexes of capacitive six-axis force sensor.

	F _x	F _y	F _z	M _x	M _y	M _z
Linearity Error	0.93 %	2.01 %	0.62 %	1.76 %	1.52 %	1.58 %
	F_x	~	1.21 %	0.79 %	1.51 %	1.62 %
	F_y	1.21 %	~	1.58 %	0.64 %	0.99 %
	F_z	1.09 %	2.01 %	~	1.37 %	1.29 %
	M_x	0.74 %	1.41 %	0.63 %	~	0.68 %
	M_y	1.74 %	0.48 %	1.25 %	1.11 %	~
Interference Error	M_z	1.95 %	1.93 %	0.64 %	1.39 %	1.53 %
						~

found to be 1.70 % of the full-scale force/torque range. With regard to the static accuracy, it was greatly improved than that of previous

studies [9,29]. As for the commercial capacitive six-axis force sensor (DynPick: WEF-6A1000-30 series), its maximum linearity error is 3.00 % F.S. and the maximum interference error can reach 5.00 % F.S. [26]. The results of the static load test demonstrated that the developed six-dimensional force sensor shows a higher measuring accuracy in comparison with commercial capacitive six-axis force sensor.

4.4. Performance evaluation

After calibration, to assess the accuracy of the prototype sensor, an evaluation setup was specially designed. As depicted in Fig. 17, it consists of a gripper exposed to the six-dimensional force, the prototype sensor and a commercial sensor (SRI-M3703C, Sunrise Instruments) as a reference for the forces and torques. Furthermore, a jig was used to connect the reference sensor and the prototype sensor. External load in an arbitrary direction was applied to the gripper. These two sensors recorded the data synchronously. During the test, the sampling frequency of data was 100 Hz. Specifically, random forces within the sensing range were applied to the gripper manually. This was different from the calibration test because the applied load included the force components in non-sensitive directions. The measured forces were calculated based on the capacitive

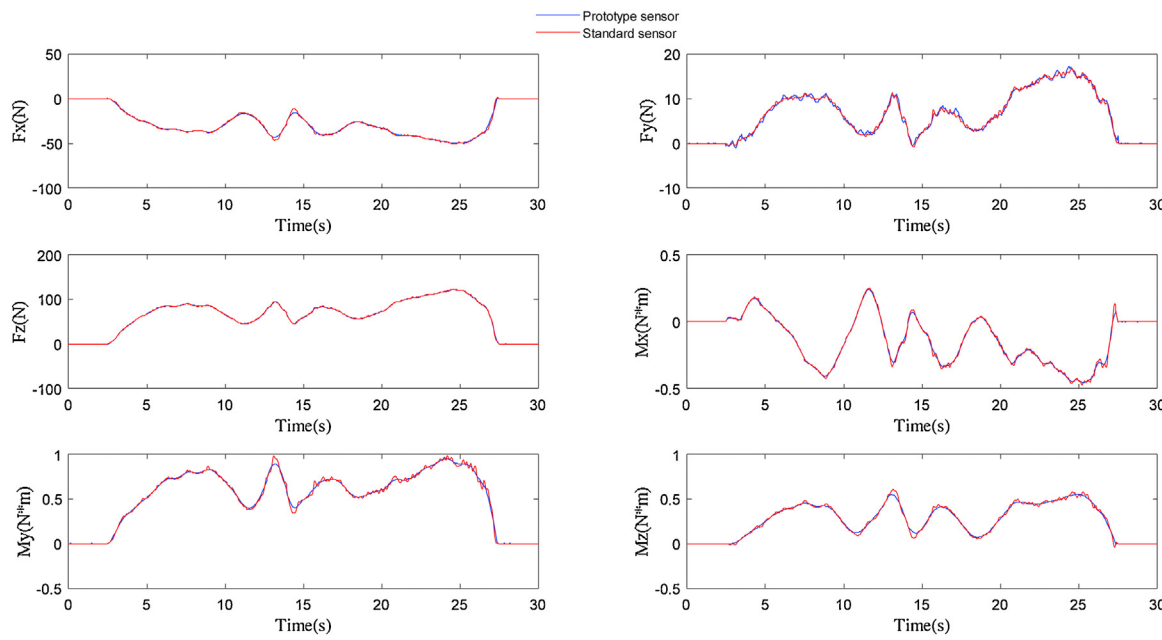


Fig. 18. Experimental results of the six-dimensional force measured by the reference sensor and the prototype.

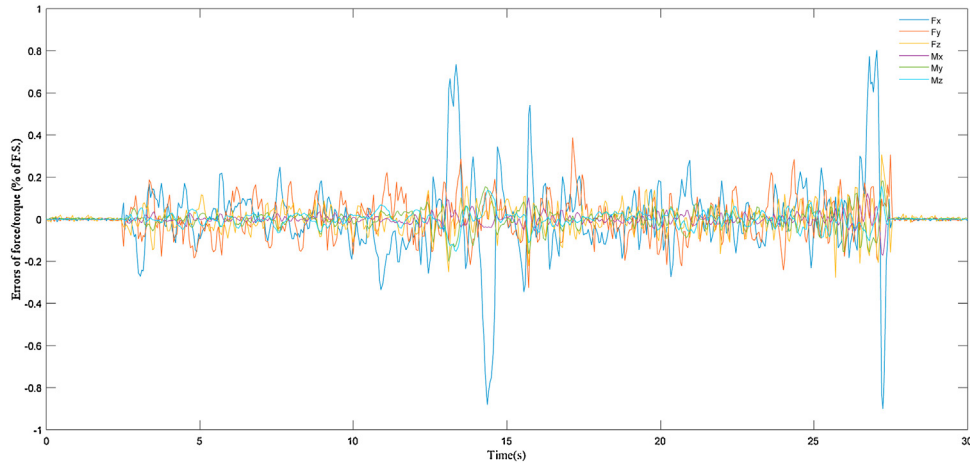


Fig. 19. Relative errors of the measured six-dimensional force in full scale sensing ranges.

data and the obtained calibration matrix. And the data acquired by the custom sensor and the reference sensor was processed offline using MATLAB. Meanwhile, the z-directional offset between these two sensors was accounted for while comparing the two sets of force components measured from them. Fig. 18 represents the time-domain responses of each axis over a period of 30 s. The red curves represent the six-axis forces measured by the reference sensor, and the blue curves denote the forces measured by the developed one. As can be seen, the experimental results show that the overall responses of both sensors were well-matched. Based on these experimental results, the average relative errors of the measured forces (F_x , F_y , F_z) are 0.36 %, 0.22 %, and 0.12 % of full scale force ranges, and the maximum errors are 0.80 %, 0.39 %, and 0.31 %. The mean values of the relative errors of the measured torques (M_x , M_y , M_z) correspond to 0.04 %, 0.12 %, and 0.07 % of full scale torque ranges, and the maximum errors are 0.12 %, 0.18 %, and 0.16 %. The errors of the forces and the torques are illustrated in Fig. 19. Thus, the feasibility of the developed sensor is validated by the well-matched two sensor's data and the phenomena. In comparison with the sensors presented in the studies [4,23], the relative

errors of the measured forces and torques in our work were significantly reduced. In addition, the average SNR during such a dynamic load test is 62.65 dB (SD 0.33 dB). The experiment verifies that the sensor system is able to output capacitive signal with a high signal to noise ratio.

4.5. Analysis of offset repeatability and time drift

To evaluate the offset repeatability of the prototype sensor, the 3-axis force (F_x , F_y , F_z) and 3-axis moment (M_x , M_y , M_z) were applied in sequence by using the load/unload method. By means of the calibration setup, the single directional force was gradually applied and released in each axis, respectively. Meanwhile, the variation curve of the capacitance was observed by recording the raw signals during the experiment. Fig. 20 shows that the prototype sensor was repeated loading and unloading cycle six times in each direction. The capacitance values were collected at each cycle in each direction. Here, the capacitance curve of the normal force sensing cell was presented. The capacitance stayed at the initial value within an acceptable range (1.541 pF). The amount of the capaci-

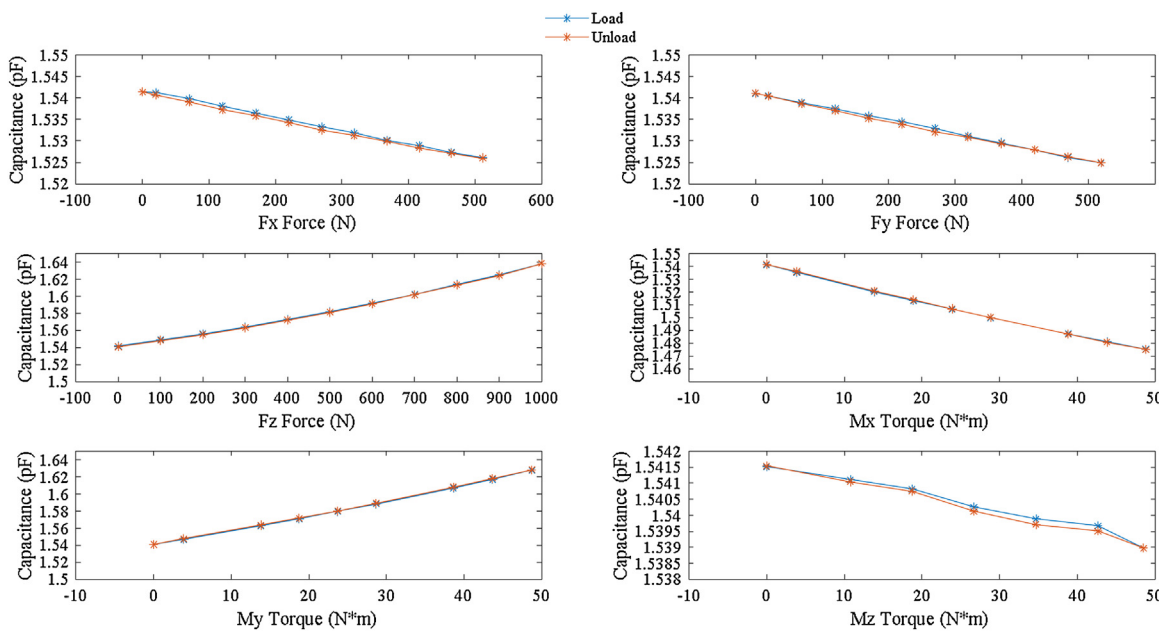


Fig. 20. The capacitance curve of the force sensing cell during the load test.

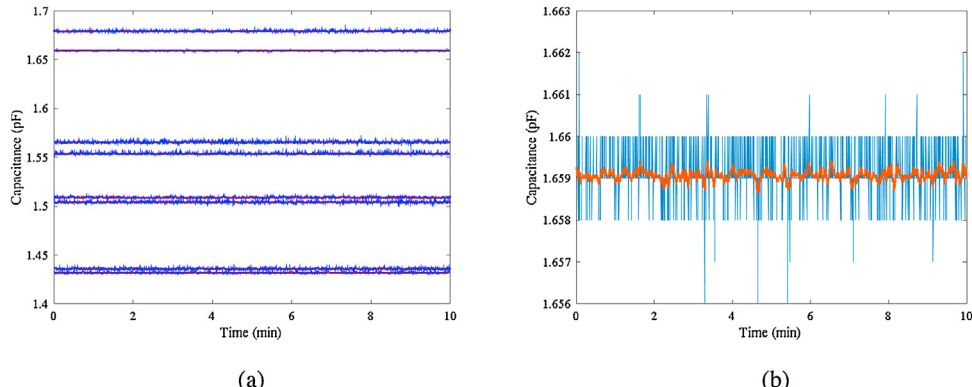


Fig. 21. Time drift of the raw capacitance signals during the ten minutes. Raw signals and filtered signals are shown in blue and red. (a) Raw capacitance signals of the prototype sensor. (b) Typical signal of the prototype sensor (Enlarged View).

tance change was not more than 0.0008 pF. It demonstrated that the capacitance initial value was repeatable in the allowed error range after repeated loading cycles.

The drift phenomenon of the prototype sensor was quantified by recording the raw capacitance signals for 10 min during experiment. The temperature variation range of the room was adjusted within 7 degrees. The filtered signals were obtained by applying moving average filter to the raw capacitance signals. Raw signals and filtered signals are shown in blue and red. As shown in Fig. 21(b), it appears that there were no significant drifts after 10 min. The capacitance was nearly maintained at 1.659 pF. The amount of the capacitance change was not more than 0.001 pF. The drift phenomenon was not obvious caused by temperature changes in the room environment of the sensor.

5. Testing on a collaborative robot (a controlled lab test)

For the collaborative robots to perform human tasks, the ability to sense the six-dimensional force is fundamental for their interaction with humans even when other sensing modalities are available. Six-axis force sensors can be of great help to robots for performing manipulation tasks. In this section, our motivation is

to validate the prototype sensor in a simulated scenario with the Baxter robot, a collaborative robot. As shown in Fig. 22, the prototype sensor was installed between the gripper and robot arm of the Baxter robot, which also has a standard commercial sensor (SRI-M3703C, Sunrise Instruments) mounted on the robotic manipulator through jigs. Experiments were conducted by handling the grasper to move in arbitrary directions in large amounts. During the experiment, the measurements with the prototype sensor and reference sensor were conducted to monitoring the variation of force simultaneously. The sensing data sampling frequency was 100 Hz. Fig. 23 shows the measured six-axis force components over a period of 30 s. The verification was performed by comparing the force data measured by the two sensors. Good match between the responses of the two sensors was found. The average relative errors of the measured forces (F_x , F_y , F_z) are 0.10 %, 0.05 %, and 0.08 % of full scale force ranges, and the maximum errors are 0.75 %, 0.44 %, and 0.59 %. The mean values of the relative errors of the measured torques (M_x , M_y , M_z) correspond to 0.03 %, 0.05 %, and 0.04 % of full scale torque ranges, and the maximum errors are 0.33 %, 0.57 %, and 0.30 %. The results exhibit the comparable sensing capability of the prototype for measuring interaction forces between the robot and human in the unstructured environment.

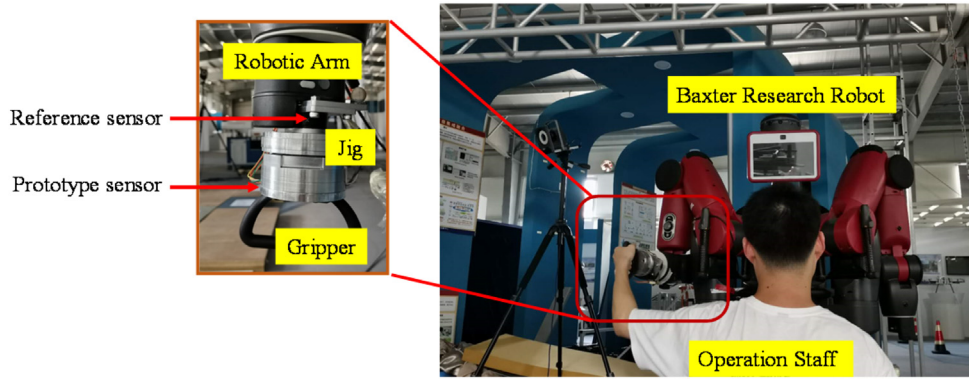


Fig. 22. Experimental images of a controlled lab test using the Baxter Research Robot.

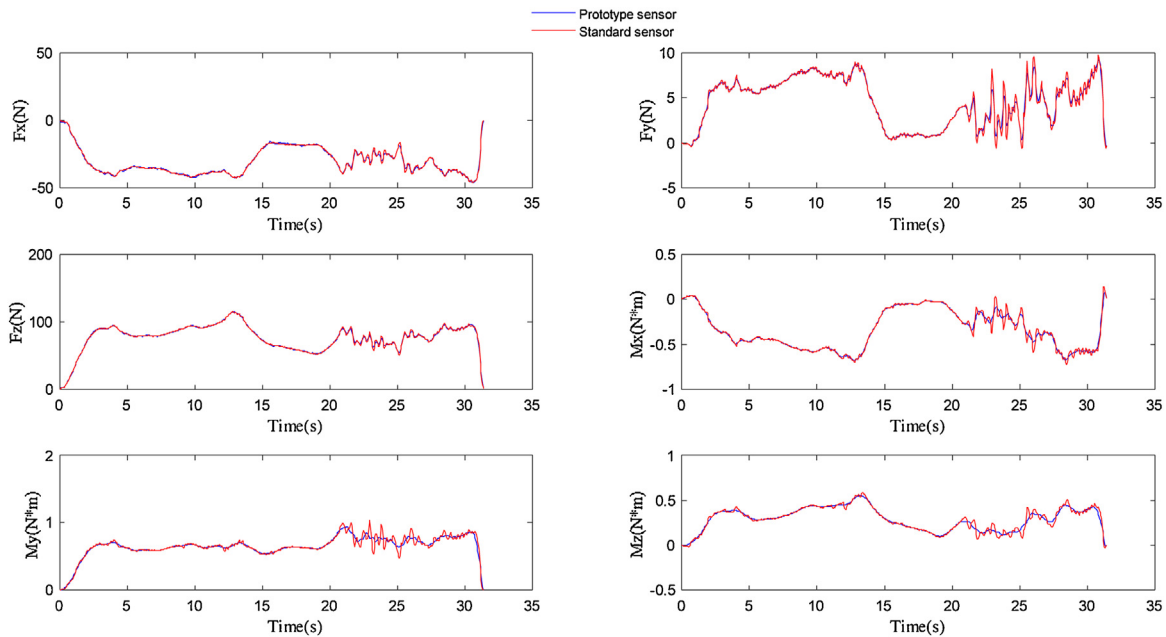


Fig. 23. Experimental results of the six-dimensional force measured by the prototype sensor and the reference sensor in a simulated scenario.

6. Conclusion

In this paper, a novel spatial configuration of the capacitor towards the six-axis force sensor was proposed. The 3D capacitor structure with a cross-shape configuration of the shear force sensing cell was designed to achieve a better decoupling effect and overall system sensitivity. Eight electrodes were arranged on three perpendicular planes of the Cartesian coordinate system independently. The six-axis force sensing capability is performed by eight capacitive sensing cells. In this configuration, the cross-shape configuration of positive electrodes for the shear force sensing was designed to reduce the coupling effect. Particularly, shear force sensing function was achieved by using a differential capacitance sensor. It provided a high sensitivity along the shear force direction, which can help to optimize overall system sensitivity with respect to the six directions. A monolithic spatial structure was manufactured with this POM material using CNC technology, and then positive electrodes were implemented with the spraying technology. Using this method, all the sensing elements can be fabricated on a single spatial structure, and manual tasks, such as bonding the sensing elements, can be eliminated. The entire manufacturing process of this sensor requires no highly elaborated manual work, which enables ease of manufacturing and reduces its production

costs. As a result, the proposed sensor is cost-effective. The manufacturing cost of the sensor is about \$300. In comparison with the commercial sensors of the similar specification (ATI Mini45), the cost has fallen dramatically.

Through various experiments, the performances of the prototype sensor are verified in terms of linearity, interference error, hysteresis, time domain response, SNR, offset repeatability and time drift. From the experimental results, the prototype sensor showed improved static accuracy than that of the previous studies [9,29]. It also demonstrated that this sensor has a higher measurement accuracy in comparison with commercial capacitive six-axis force sensor [26]. As for the dynamic loading test, the measured forces and torques in our work had smaller relative errors in comparison with the sensors presented in previous study [4,23]. The results exhibit the comparable sensing capability of the low-cost prototype for measuring the physical interaction forces in the unstructured environment. The proposed structure shows potential to achieve an ideal isotropic property even in a larger moment to force ratio. As an extension to the current work, in order to improve the isotropic property and sensing accuracy further, more elaborated optimization design methods are required to explore. Future studies aim to miniaturize the sensor and optimize its core geometric dimensioning for the best performance. Then, the force

feedback control experiment in an actual robotic system using this six-axis force sensor should be conducted to verify its performance. The capacitive sensing technology used in the sensor holds great potential for applications in a wide variety of robotic applications.

CRediT authorship contribution statement

Zexia He: Conceptualization, Methodology, Formal analysis, Investigation, Writing - original draft, Writing - review & editing.
Tao Liu: Conceptualization, Formal analysis, Resources, Writing - review & editing, Supervision.

Declaration of Competing Interest

The authors report no declarations of interest.

Acknowledgments

This work was supported in part by the NSFC Grant No. 51775485, and the Zhejiang Provincial Natural Science Foundation of China under Grant No. LZ20E050002.

References

- [1] A.F. Azocar, L.M. Mooney, J.-F. Duval, A.M. Simon, L.J. Hargrove, E.J. Rouse, Design and clinical implementation of an open-source bionic leg, *Nat. Biomed. Eng.* (2020).
- [2] Y.P. Shi, P.F. Wang, X. Wang, F.S. Zha, Z.Y. Jiang, W. Guo, et al., Bio-inspired equilibrium point control scheme for quadrupedal locomotion, *IEEE Trans. Cogn. Dev. Syst.* 11 (2019) 200–209.
- [3] H. Su, C.G. Yang, G. Ferrigno, E. De Momi, Improved human-robot collaborative control of redundant robot for teleoperated minimally invasive surgery, *IEEE Robot. Autom. Lett.* 4 (2019) 1447–1453.
- [4] U. Kim, Y.B. Kim, D.Y. Seok, J. So, H.R. Choi, A surgical palpation probe with 6-axis force/torque sensing capability for minimally invasive surgery, *IEEE Trans. Ind. Electron.* 65 (2018) 2755–2765.
- [5] L. Gabert, I. Lenzi, Instrumented pyramid adapter for amputee gait analysis and powered prosthesis control, *IEEE Sens. J.* 19 (2019) 8272–8282.
- [6] U. Kim, D.H. Lee, W.J. Yoon, B. Hannaford, H.R. Choi, Force sensor integrated surgical forceps for minimally invasive robotic surgery, *IEEE Trans. Robot.* 31 (2015) 1214–1224.
- [7] J.O. Templeman, B.B. Sheil, T. Sun, Multi-axis force sensors: a state-of-the-art review, *Sens. Actuators A-Phys.* 304 (2020) 17.
- [8] ATI Industrial Automation Inc, Multi-Axis Force/Torque Sensor, 2013 <https://www.ati-ia.com/>.
- [9] D.H. Lee, U. Kim, H. Jung, H.R. Choi, A capacitive-type novel six-axis force/torque sensor for robotic applications, *IEEE Sens. J.* 16 (2016) 2290–2299.
- [10] J. Ma, A. Song, Fast estimation of strains for cross-beams six-axis force/torque sensors by mechanical modeling, *Sensors* 13 (2013) 6669–6686.
- [11] D. Okumura, S. Sakaino, T. Tsuji, High dynamic range sensing by a multistage six-axis force sensor with stopper mechanism, in: 2018 IEEE International Conference on Robotics and Automation, IEEE Computer Soc, Los Alamitos, 2018, pp. 4065–4070.
- [12] B. Wu, J. Luo, F. Shen, Y. Ren, Z. Wu, Optimum design method of multi-axis force sensor integrated in humanoid robot foot system, *Measurement* 44 (2011) 1651–1660.
- [13] M.K. Kang, S. Lee, J.H. Kim, Shape optimization of a mechanically decoupled six-axis force/torque sensor, *Sens. Actuators A-Phys.* 209 (2014) 41–51.
- [14] L.Y. Fu, A.G. Song, D.P. Chen, A polyetheretherketone six-axis force/torque sensor, *IEEE Access* 7 (2019) 105391–105401.
- [15] H. Akbari, A. Kazerouni, Improving the coupling errors of a Maltese cross-beams type six-axis force/moment sensor using numerical shape-optimization technique, *Measurement* 126 (2018) 342–355.
- [16] Y.J. Li, B.Y. Sun, J. Zhang, M. Qian, Z.Y. Jia, A novel parallel piezoelectric six-axis heavy force/torque sensor, *Measurement* 42 (2009) 730–736.
- [17] Y.J. Li, J. Zhang, Z.Y. Jia, M. Qian, A novel piezoelectric 6-component heavy force/moment sensor for huge heavy-load manipulator's gripper, *Mech. Syst. Signal Proc.* 23 (2009) 1644–1651.
- [18] Y.J. Li, G.C. Wang, J. Zhang, Z.Y. Jia, Dynamic characteristics of piezoelectric six-dimensional heavy force/moment sensor for large-load robotic manipulator, *Measurement* 45 (2012) 1114–1125.
- [19] J.T. Yao, J.L. Zhu, Z.J. Wang, Y.D. Xu, Y.S. Zhao, Measurement theory and experimental study of fault-tolerant fully pre-stressed parallel six-component force sensor, *IEEE Sens. J.* 13 (2013) 3472–3482.
- [20] Z.J. Wang, Z.X. Li, J. He, J.T. Yao, Y.S. Zhao, Optimal design and experiment research of a fully pre-stressed six-axis force/torque sensor, *Measurement* 46 (2013) 2013–2021.
- [21] Z.-Y. Jia, S. Lin, W. Liu, Measurement method of six-axis load sharing based on the Stewart platform, *Measurement* 43 (2010) 329–335.
- [22] R. Bekhti, V. Duchaine, P. Cardou, Ieee, miniature capacitive three-axis force sensor, 2014 Ieee/Rsj International Conference on Intelligent Robots and Systems (2014) 3939–3946.
- [23] U. Kim, D.H. Lee, Y.B. Kim, D.Y. Seok, H.R. Choi, A novel six-axis force/torque sensor for robotic applications, *IEEE ASME* 22 (2017) 1381–1391.
- [24] Y.B. Kim, U. Kim, D.Y. Seok, J. So, Y.H. Lee, H.R. Choi, Torque sensor embedded actuator module for robotic applications, *IEEE-ASME Trans. Mechatron.* 23 (2018) 1662–1672.
- [25] H.S. Oh, U. Kim, G. Kang, J.K. Seo, H.R. Choi, Multi-axial force/torque sensor calibration method based on deep-learning, *IEEE Sens. J.* 18 (2018) 5485–5496.
- [26] WACOH-TECH Inc, DynPick: WEF-6A1000-30 Series <https://wacoh-tech.com/products/dynpick/>.
- [27] A. Bicchi, A criterion for optimal design of multi-axis force sensors, *Rob. Auton. Syst.* 10 (1992) 269–286.
- [28] M. Uchiyama, Y. Nakamura, K. Hakomori, Evaluation of the robot force sensor structure using singular value decomposition, *Adv. Robot.* 5 (1990) 39–52.
- [29] D. Kim, C.H. Lee, B.C. Kim, D.H. Lee, H.S. Lee, N. Canh Toan, et al., Six-axis capacitive force/torque sensor based on dielectric elastomer, in: Y. BarCohen (Ed.), *Electroactive Polymer Actuators and Devices*, 2013.

Biographies



Zexia He received the M.S. degree in mechanical engineering from Dalian University of Technology, Dalian, China, in 2016. He is currently pursuing the Ph.D. degree in the State Key Laboratory of Fluid Power and Mechatronic Systems, School of Mechanical Engineering, Zhejiang University, since 2016. His current research interests include multi-axis force sensing system, tactile sensors and wearable sensor system for robot applications.



Tao Liu (M'08–SM'15) received the M.Eng. degree in mechanical engineering from the Harbin Institute of Technology, Harbin, China, in 2003, and the Ph.D. degree in engineering from the Kochi University of Technology, Kochi, Japan, in 2006. Tao Liu (M'08–SM'15) received the M.Eng. degree in mechanical engineering from the Harbin Institute of Technology, Harbin, China, in 2003, and the Ph.D. degree in engineering from the Kochi University of Technology, Kochi, Japan, in 2006. He has been an Assistant Professor with the Department of Intelligent Mechanical Systems Engineering, Kochi University of Technology, from 2009 to 2013. He is currently a Professor with the State Key Laboratory of Fluid Power and Mechatronic Systems, and the Director of the Department of Mechanical Engineering, Institute of Micro-/Nanotechnology and Precision Engineering, Zhejiang University, China. His current research interests include wearable sensor systems, rehabilitation robots, biomechanics, and human motion analysis.